

In situ control of effective Kerr nonlinearity with Pockels integrated photonics

Nanophotonic cavities with Kerr nonlinearities are a versatile platform both to explore fundamental physics and to develop practical photonic technologies¹⁻³. This is possible because nanoscale structures allow precise dispersion control and provide significant field enhancement. To improve the functionality and performance of photonic devices even further, direct control of the Kerr nonlinearity would be desirable. Here, we report the in situ control of integrated Kerr nonlinearity through its interplay with the cascaded second-order nonlinear process⁴⁻⁹. We observe a Fano resonance in the nonlinear spectrum rather than in the linear transmission¹⁰, confirming the quantum interference between competing optical nonlinear pathways. The Kerr nonlinearity is tuned over a dynamic range of 10 dB without modifying the photonic structure. We also demonstrate the suppression of the intrinsic material nonlinearity and we use the tunable nonlinearity to control the spectral brightness and coincidence-to-accidental ratio of single-photon generation.

The dynamic control of optical properties plays an indispensable role in a great number of fields. The linear optical properties such as refractive index and absorption can be modified in nanophotonic circuits using a wide variety of phenomena including thermal¹¹, electrical^{12,13}, mechanical¹⁴ and free-carrier effects¹⁵. This allows the modulation of optical fields with broad applications ranging from laser systems to optical communications. Recently, such linear control has also been used to demonstrate functions including the reconfigurable generation of topological photonic states^{16,17}, the photonic acceleration of machine learning algorithms^{18,19} and the realization of universal photonic quantum gates^{20,21}.

Similarly, the control of optical nonlinear properties will lead to significant scientific and technological advances. The enhancement of nonlinearity can obviously benefit broad photonic technologies including all-optical information processing^{22–24}, quantum computing²⁵⁻²⁸, temporal-frequency conversion²⁹⁻³¹ and so on. The full coherent control of nonlinearity beyond simple enhancement can further expand the scope of photonic technology. The nonlinearity suppression is critical to fundamentally improve the sensitivity of optical sensors^{32,33} and the capacity of optical communications^{34,35}. The phase inversion of the nonlinear interaction can enable the generation of unconventional soliton states^{36,37}. Currently, nanophotonic nonlinear processes are only controlled indirectly using intra-cavity photon number and dispersion. Therefore, the achievable nonlinearity and functionality are limited to the intrinsic property of the material at specific wavelengths. Cascaded second-order nonlinearity has been demonstrated as an efficient method to increase the effective third-order strength^{38–46}. The simultaneous implementation and coherent control of the cascaded second-order and third-order nonlinearities can further expand the capability of photonic devices⁷⁻⁹. Such advanced

functions can only be realized by integrated photonic platforms with second-order nonlinearity 47,48 .

In this Letter, we demonstrate a method to control the effective Kerr nonlinearity in integrated photonic cavities without modifying the photonic structure. By designing its interference with cascaded Pockels processes, the complete amplitude and phase control of effective Kerr nonlinearity can be realized in a nanophotonic cavity. Besides the enhancement of Kerr nonlinearity, we also observe effects including the nonlinearity suppression and Fano resonances in the nonlinear regime. The effective Kerr nonlinearity is highly tunable over 10 dB dynamic range with fixed photonic structures. We further validate the control of Kerr nonlinearity in both the classical and quantum regimes through nonlinear frequency conversion and single-photon generation.

In the degenerate configuration of Kerr nonlinear processes, two pump photons are annihilated to generate one signal and one idler photon, or vice versa (Fig. 1a). The nonlinearity is fixed by the material property and photonic structure. To modify the Kerr nonlinearity, we design a cascaded Pockels nonlinear process shown in Fig. 1b. In this process, two pump photons first combine into one photon through second-harmonic generation (SHG). Then the second-harmonic photon drives the parametric down-conversion (PDC) process in the same photonic cavity to generate one signal and one idler photon. The effective interaction Hamiltonian for the cascaded Pockels nonlinear process is

$$H_{\rm I} = -\frac{1}{2} \hbar (g_{\rm c} \hat{b}_{\rm p}^{\dagger 2} \hat{b}_{\rm s} \hat{b}_{\rm i} + g_{\rm c}^* \hat{b}_{\rm p}^2 \hat{b}_{\rm s}^{\dagger} \hat{b}_{\rm i}^{\dagger}) \tag{1}$$

with $\hat{b}_{\rm p}$, $\hat{b}_{\rm s}$ and $\hat{b}_{\rm i}$ the annihilation operators of the pump, signal and idler modes respectively (Supplementary Section I). The effective cascaded Pockels nonlinear strength $g_{\rm c}$ at single-photon level is defined as

$$g_{\rm c} = \frac{-\mathrm{i}|g_2|^2}{\mathrm{i}\Delta + \gamma/2} \tag{2}$$

with g_2 the Pockels nonlinear strength, Δ the frequency difference between twice the pump frequency and the second-harmonic mode, and γ the decay rate of the second-harmonic mode. This interaction Hamiltonian has the same form as intrinsic Kerr nonlinear processes. With highly efficient Pockels nonlinear processes, the effective Kerr nonlinearity can be significantly enhanced.

To implement the cascaded Pockels nonlinear process, we use a nanophotonic ring cavity made of aluminum nitride (Fig. 2a). The phase-matching condition for the Pockels nonlinear process is satisfied using a high-order transverse-magnetic (TM) second-harmonic mode and a fundamental TM pump mode (Supplementary Section II). Strong second-harmonic generation

LETTERS NATURE PHYSICS

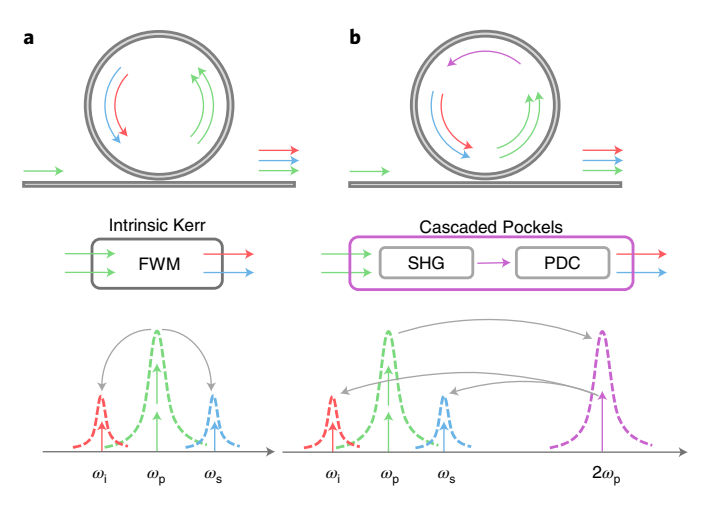


Fig. 1| Effective Kerr nonlinearity with cascaded Pockels process.

a, Intrinsic Kerr process. Two pump photons are annihilated to generate one signal and one idler photon. **b**, Cascaded Pockels process. Two pump photons are annihilated to generate one second-harmonic photon, which drives the parametric down-conversion to generate one signal and one idler photon. PDC, parametric down conversion; SHG, second-harmonic generation. ω_p , ω_s , and ω_l are the the pump, signal, and idler angular frequency respectively.

is observed with a pump wavelength near 1,518 nm (Fig. 2b). The second-harmonic generation efficiency is measured as $\eta \approx 1,800\%$ per Watt, leading to the estimated Pockels nonlinear strength $g_2 \approx 2\pi \times 81\,\mathrm{kHz}$ (Supplementary Section II). With the small decay rate of the second-harmonic mode ($\gamma \approx 2\pi \times 4.5\,\mathrm{GHz}$), we can expect the enhanced Kerr nonlinearity around $|g_c| \approx 2\pi \times 3\,\mathrm{Hz}$ at zero frequency detune, which is sixfold higher than the intrinsic value ($g_3 \approx 2\pi \times 0.5\,\mathrm{Hz}$).

The enhancement of the Kerr nonlinearity is first verified with stimulated four-wave mixing (FWM) for frequency conversion in the classical domain. With a strong pump (P_p) , we measure the conversion from the idler input (P_i) to the signal output (P_s) . We use two sets of modes from the same nanophotonic cavity to measure the intrinsic and enhanced Kerr nonlinearity respectively. The pump mode of the reference set is not phase-matched to the Pockels nonlinear process. Therefore, only the intrinsic Kerr nonlinearity contributes to the nonlinear frequency conversion. The pump mode of the other set is phase-matched to the Pockels nonlinear process. As a result, the enhanced Kerr nonlinearity dominates the nonlinear frequency conversion. The two sets of modes share similar quality factors and coupling conditions. Consequently, the influence of different cavity-enhancement factors and extraction efficiencies can be eliminated (Supplementary Section II). The generation of the signal field is observed from the output optical spectrum with both mode sets (Fig. 2c). Comparing the two mode sets, the signal output of the phase-matched set is significantly higher than that of the reference set, even though smaller pump and idler inputs are used. To calibrate the enhancement factor, we fix the input idler power (P_i) and vary the input pump power (P_p) . To achieve the same signal output (P_s) , the cascaded Pockels nonlinear process uses 7.5 dB less pump power than the intrinsic Kerr nonlinearity (Fig. 2d). This agrees well with the difference between the enhanced and intrinsic Kerr nonlinearity ($|g_c/g_3| \approx 6$). The critical role of the Pockels nonlinear process is further confirmed by the increased second-harmonic generation with respect to the pump power (Fig. 2d). The same conclusion is obtained from the measurement with different input idler power (P_i) . With the same pump power, the cascaded Pockels process can generate approximately 15 dB stronger signal output.

The second-harmonic generation remains constant during the process, which confirms that the second-harmonic field is generated from the pump.

The coherent interaction between multiple nonlinear processes can be used to tune the overall nonlinear response. This enables the complete control over the amplitude and phase of the effective Kerr nonlinearity. Taking both the intrinsic Kerr strength g_3 and cascaded Pockels nonlinear rate g_c into account (Fig. 3a), the effective Kerr nonlinearity can be written as

$$g_{\text{eff}} = g_3 + g_c = g_3 - \frac{i|g_2|^2}{i\Delta + \frac{\gamma}{2}}.$$
 (3)

The relative phase φ between the two nonlinear processes can be controlled by the frequency detune Δ (Fig. 3b). Both constructive and destructive interference can be realized, leading to the enhancement and suppression of the effective Kerr nonlinearity, respectively (Fig. 3c). Here, we define

$$\xi = |g_2|^2 / g_3 \gamma \tag{4}$$

so that 2ξ is the relative strength between the two nonlinear processes at zero frequency detune. The maximum and minimum

effective nonlinearity
$$|g_{\text{max/min}}| = g_3 \left(\frac{\sqrt{1+\xi^2}\pm\xi}{\sqrt{1+\xi^2}\mp\xi}\right)^{1/2}$$
 can be obtained

at frequency detunes $\Delta = \frac{\gamma}{2}(\xi \mp \sqrt{1+\xi^2})$. Therefore, a larger tuning dynamic range can be achieved with more efficient Pockels nonlinear processes (Fig. 3d).

To verify the quantum interference between the cascaded Pockels and the intrinsic Kerr nonlinear processes, we perform single-photon generation with spontaneous FWM. The frequency detune Δ is precisely controlled through the device temperature (Supplementary Section II). The pump light is tuned in resonance with the pump mode to ensure that the intra-cavity pump photon number remains constant. The single-photon generation rate of the signal channel (proportional to $|g_{eff}|^2$) is recorded to infer the effective Kerr nonlinearity. We use two different Pockels nonlinear strengths corresponding to $\xi = 0.14$ and $\xi = 0.92$ respectively by selecting two different phase-matching modes (Supplementary Section II). The single-photon count rate shows Fano lineshape in both cases (Fig. 4a,c), indicating the coherent interaction between two competing optical nonlinear processes. A larger tuning dynamic range of the Kerr nonlinearity is achieved with the stronger Pockels nonlinear strength ($\pm 0.6 \, dB$ with $\xi = 0.14 \, versus \, \pm 3.6 \, dB$ with $\xi = 0.92$), which matches our theoretical model (Fig. 3c). As a reference, we also measure the single-photon generation rate of the same signal channel with parametric down-conversion by pumping a visible laser into the cavity under different frequency detune (Fig. 4b,d), which shows Lorentzian lineshape. This confirms the quantum interference between the broad-band intrinsic Kerr process and the narrow-band cascaded Pockels nonlinear process. It is noteworthy that Fano resonances in our experiment can only be observed with a nonlinear spectrum, as the interference happens between nonlinear processes. This is in contrast to Fano resonances introduced by linear coupling between resonators, where linear transmission is sufficient to observe the asymmetric lineshape⁸.

Finally, we demonstrate the control of the coincidence-to-accidental ratio (CAR) of the single-photon generation by changing the effective Kerr nonlinearity. The CAR is a critical parameter to characterize the quality of single photon sources. In the low pump regime, background noise and a leaking pump dominate the noise photon count. Therefore, the CAR can be improved by increasing the pump power. In the high pump regime, multi-photon generation becomes the major noise source. As a result, the CAR drops with increased pump power.

NATURE PHYSICS LETTERS

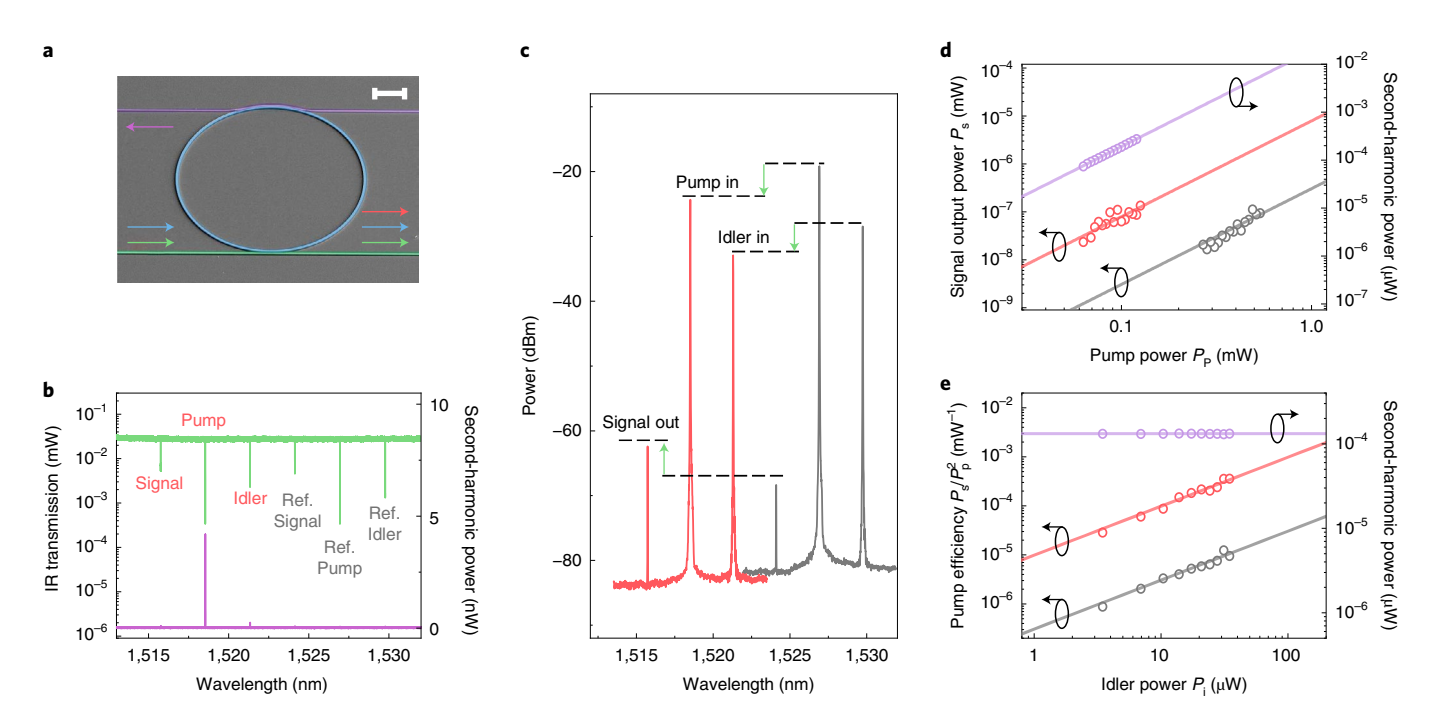


Fig. 2 | Enhancement of Kerr nonlinearity. a, Scanning electron microscope image of the fabricated aluminum nitride device with the ring cavity (blue), the bus waveguide for second-harmonic field (purple) and the bus waveguide for pump, idler and signal fields (green). Scale bar, 20 μm. **b**, Pump transmission (green) and second-harmonic (purple) spectrum. Two sets of modes for FWM, with (red) and without (grey) Pockels phase-matching, are labelled. **c**, The output optical spectrum of the stimulated FWM. **d**, The output signal (red and grey) and second-harmonic power (purple) with different pump power. **e**, The pump efficiency (red and grey) and second-harmonic power (purple) with different idler input power. Results in **c**, **d** and **e** using the reference mode set and the mode set with Pockels phase-matching are presented in red and grey, respectively. Experimental data (circles) are fitted with the theoretical model (solid lines).

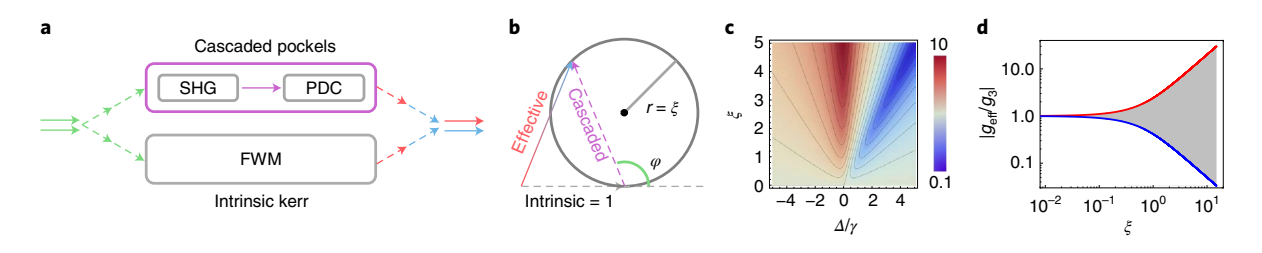


Fig. 3 | Quantum interference between nonlinear processes. a, Schematic for the quantum interference between intrinsic Kerr and cascaded Pockels processes. **b**, Vector diagram showing the coherent interaction between the intrinsic Kerr and cascaded Pockels processes. Phase φ can be controlled by the frequency detune Δ. Intrinsic Kerr nonlinearity is normalized to 1 and the tuning range of the effective Kerr nonlinearity is bounded to the circle with radius ξ. **c**, Calculated effective Kerr nonlinearity $|g_{eff}/g_3|$ in logarithm scale from 0.1 (blue) to 10 (red). **d**, Calculated maximum and minimum effective Kerr nonlinearity. The shaded area indicates the accessible range of the effective Kerr nonlinearity. PDC, parametric down conversion; SHG, second-harmonic generation.

We first set the frequency detune $\Delta=2\pi\times1.5\,\mathrm{GHz}$ with $\xi=0.92$ to achieve the maximum nonlinearity suppression (blue point in Fig. 4c). We measure the cross-correlation between signal and idler photons ($g^{(2)}$) to extract the dependence of the CAR on the pump power (Fig. 4f,g). The maximum CAR of 9 ± 1 is achieved using 3 dBm pump power. Next, we set the frequency detune $\Delta=-2\pi\times0.7\,\mathrm{GHz}$ to realize the maximum nonlinearity enhancement (red point in Fig. 4c). The maximum achievable CAR is 47 ± 2 with -2 dBm pump power, corresponding to more than five-fold improvement. We also calibrated photon rates of the background noise, pump-induced noise and parametric photon pairs (Fig. 4e) to directly calculate the CAR, which agrees with the result obtained from the coincidence measurement (Fig. 4f and Supplementary Section III).

We have demonstrated the quantum-level coherent interaction between intrinsic Kerr and cascaded Pockels processes, leading to the in situ control of effective Kerr nonlinearity. This scheme can be readily implemented with other integrated photonic platforms with second-order nonlinearity^{48–50}. In particular, the recent development of thin-film lithium niobate photonic devices can significantly increase the strength of the cascaded Pockels process. With the large Pockels coefficient (30 pm V $^{-1}$) and small visible cavity loss ($\gamma < 2\pi \times 40 \, \text{MHz})^{51}$, the effective Kerr nonlinearity can reach megahertz level with similar device sizes. Given that lithium niobate photonic cavities can reach linewidths below 10 MHz with telecom wavelengths^{48,52}, our scheme could lead to the demonstration of a single-photon strong coupling regime with Kerr nonlinearity, enabling deterministic quantum logic operations with

LETTERS NATURE PHYSICS

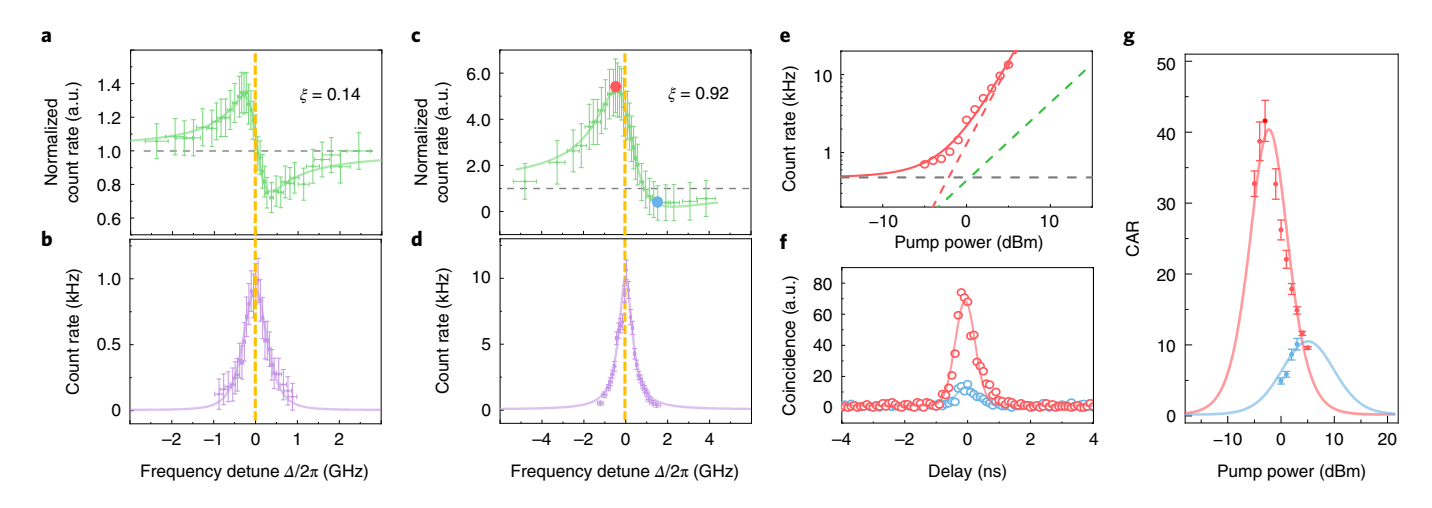


Fig. 4 | Continuous tuning of Kerr nonlinear strength in the quantum regime. a,c, Single-photon generation rate from spontaneous FWM using effective Kerr nonlinearity with $\xi=0.14$ and $\xi=0.92$, respectively. The data are normalized to the count rate with the intrinsic Kerr nonlinearity (grey dashed line), and the arbitrary unit (a.u.) is used. **b,d**, Single-photon generation rate from spontaneous parametric down-conversion with $\xi=0.14$ and $\xi=0.92$, respectively. **e**, Single-photon generation rate (red circles) with different pump power. Calculated background dark count (black dashed line), pump-induced noise (green dashed line), signal photon rate (red dashed line) and total photon rate (red solid line) are plotted. All photon counting data are measured from the signal resonance. **f**, Signal-idler coincidence count with frequency detune $\Delta=-2\pi\times0.7$ GHz (red point in **c**) and $\Delta=2\pi\times1.5$ GHz (blue point in **c**). Pump power is 1 mW. The accidental coincidence outside the coherent window is normalized to 1. **g**, CARs under different pump powers with frequency detune $\Delta=-2\pi\times0.7$ GHz (red) and $\Delta=2\pi\times1.5$ GHz (blue). Points, measured CARs from signal-idler coincidence; lines, calculated CARs from calibrated signal, idler and noise photon rates.

all-photonic systems^{26–28}. While the enhancement of Kerr nonlinearity can directly find broad applications, it is also worth noting that novel functions including the suppression and phase tuning of Kerr nonlinearity could also open unique prospects for photonic technologies, such as eliminating nonlinear noise and improving the dynamic range of optical sensing and communication systems.

Online content

Any methods, additional references, Nature Research reporting summaries, source data, extended data, supplementary information, acknowledgements, peer review information; details of author contributions and competing interests; and statements of data and code availability are available at https://doi.org/10.1038/s41567-022-01542-x.

Received: 1 September 2021; Accepted: 8 February 2022; Published online: 31 March 2022

References

- Kippenberg, T. J., Gaeta, A. L., Lipson, M. & Gorodetsky, M. L. Dissipative Kerr solitons in optical microresonators. *Science* 361, eaan8083 (2018).
- Gaeta, A. L., Lipson, M. & Kippenberg, T. J. Photonic-chip-based frequency combs. Nat. Photonics 13, 158–169 (2019).
- 3. Kues, M. et al. Quantum optical microcombs. *Nat. Photonics* 13, 170–179 (2019).
- Schiek, R. Nonlinear refraction caused by cascaded second-order nonlinearity in optical waveguide structures. J. Opt. Soc. Am. B 10, 1848–1855 (1993).
- White, A., Mlynek, J. & Schiller, S. Cascaded second-order nonlinearity in an optical cavity. Europhys. Lett. 35, 425–430 (1996).
- Biaggio, I. Degenerate four-wave mixing in noncentrosymmetric materials. Phys. Rev. A 64, 063813 (2001).
- Kolleck, C. Cascaded second-order contribution to the third-order nonlinear susceptibility. Phys. Rev. A 69, 053812 (2004).
- Li, M., Zou, C.-L., Dong, C.-H. & Dai, D.-X. Optimal third-harmonic generation in an optical microcavity with χ⁽²⁾ and χ⁽³⁾ nonlinearities. *Opt. Express* 26, 27294–27304 (2018).
- Li, M., Zou, C.-L., Dong, C.-H., Ren, X.-F. & Dai, D.-X. Enhancement of second-harmonic generation based on the cascaded second-and third-order nonlinear processes in a multimode optical microcavity. *Phys. Rev. A* 98, 013854 (2018).

- Limonov, M. F., Rybin, M. V., Poddubny, A. N. & Kivshar, Y. S. Fano resonances in photonics. *Nat. Photonics* 11, 543–554 (2017).
- Harris, N. C. et al. Efficient, compact and low loss thermo-optic phase shifter in silicon. Opt. Express 22, 10487–10493 (2014).
- Wang, C., Zhang, M., Stern, B., Lipson, M. & Lončar, M. Nanophotonic lithium niobate electro-optic modulators. Opt. Express 26, 1547–1555 (2018).
- 13. Wang, C. et al. Integrated lithium niobate electro-optic modulators operating at CMOS-compatible voltages. *Nature* **562**, 101–104 (2018).
- Dong, P. et al. Low power and compact reconfigurable multiplexing devices based on silicon microring resonators. *Opt. Express* 18, 9852–9858 (2010).
- Reed, G. T., Mashanovich, G., Gardes, F. Y. & Thomson, D. Silicon optical modulators. Nat. Photonics 4, 518–526 (2010).
- Zhao, H. et al. Non-Hermitian topological light steering. Science 365, 1163–1166 (2019).
- Zhang, Z. et al. Tunable topological charge vortex microlaser. Science 368, 760–763 (2020).
- Shen, Y. et al. Deep learning with coherent nanophotonic circuits. Nat. Photonics 11, 441–446 (2017).
- Feldmann, J., Youngblood, N., Wright, C. D., Bhaskaran, H. & Pernice, W. H. All-optical spiking neurosynaptic networks with self-learning capabilities. *Nature* 569, 208–214 (2019).
- 20. Carolan, J. et al. Universal linear optics. Science 349, 711-716 (2015).
- Wang, J., Sciarrino, F., Laing, A. & Thompson, M. G. Integrated photonic quantum technologies. *Nat. Photonics* 14, 273–284 (2020).
- 22. Willner, A. E., Khaleghi, S., Chitgarha, M. R. & Yilmaz, O. F. All-optical signal processing. *J. Light. Technol.* **32**, 660–680 (2013).
- Li, M. et al. Photon-level tuning of photonic nanocavities. Optica 6, 860–863 (2019).
- Zasedatelev, A. V. et al. Single-photon nonlinearity at room temperature. Nature 597, 493–497 (2021).
- O'Brien, J. L., Furusawa, A. & Vučković, J. Photonic quantum technologies. Nat. Photonics 3, 687–695 (2009).
- Milburn, G. J. Quantum optical Fredkin gate. Phys. Rev. Lett. 62, 2124–2127 (1989).
- Brod, D. J. & Combes, J. Passive C-phase gate via cross-Kerr nonlinearities. Phys. Rev. Lett. 117, 080502 (2016).
- Heuck, M., Jacobs, K. & Englund, D. R. Controlled-phase gate using dynamically coupled cavities and optical nonlinearities. *Phys. Rev. Lett.* 124, 160501 (2020).
- Foster, M. A. et al. Silicon-chip-based ultrafast optical oscilloscope. Nature 456, 81–84 (2008).
- Fan, L. et al. Integrated optomechanical single-photon frequency shifter. Nat. Photonics 10, 766–770 (2016).

NATURE PHYSICS LETTERS

- Fan, L., Zou, C.-L., Zhu, N. & Tang, H. X. Spectrotemporal shaping of itinerant photons via distributed nanomechanics. *Nat. Photonics* 13, 323–327 (2019).
- 32. Iwatsuki, K., Hotate, K. & Higashiguchi, M. Kerr effect in an optical passive ring-resonator gyro. *J. Light. Technol.* 4, 645–651 (1986).
- 33. Liang, W. et al. Resonant microphotonic gyroscope. Optica 4, 114-117 (2017).
- 34. Ellis, A. D., Zhao, J. & Cotter, D. Approaching the non-linear Shannon limit. J. Light. Technol. 28, 423–433 (2009).
- Le, S. T., Aref, V. & Buelow, H. Nonlinear signal multiplexing for communication beyond the Kerr nonlinearity limit. *Nat. Photonics* 11, 570–576 (2017).
- Xue, X. et al. Mode-locked dark pulse Kerr combs in normal-dispersion microresonators. Nat. Photonics 9, 594–600 (2015).
- Helgason, Ó. B. et al. Dissipative solitons in photonic molecules. *Nat. Photonics* 15, 305–310 (2021).
- Bosshard, C. et al. Cascaded contributions to degenerate four-wave mixing in an acentric organic crystal. Opt. Lett. 24, 196–198 (1999).
- Tan, H.-T. & Huang, H. Bright quadripartite entanglement from competing
 γ⁽²⁾ nonlinearities. *Phys. Rev. A* 83, 015802 (2011).
- Sasagawa, K. & Tsuchiya, M. Highly efficient third harmonic generation in a periodically poled MgO:LiNbO₃ disk resonator. *Appl. Phys. Express* 2, 122401 (2009).
- Ulvila, V., Phillips, C. R., Halonen, L. & Vainio, M. Frequency comb generation by a continuous-wave-pumped optical parametric oscillator based on cascading quadratic nonlinearities. Opt. Lett. 38, 4281–4284 (2013).
- Li, G.-Z., Chen, Y.-P., Jiang, H.-W. & Chen, X.-F. Enhanced Kerr electro-optic nonlinearity and its application in controlling second-harmonic generation. *Photonics Res.* 3, 168–172 (2015).
- 43. Liu, S., Zheng, Y. & Chen, X. Cascading second-order nonlinear processes in a lithium niobate-on-insulator microdisk. *Opt. Lett.* **42**, 3626–3629 (2017).

- Wolf, R., Breunig, I., Zappe, H. & Buse, K. Cascaded second-order optical nonlinearities in on-chip micro rings. Opt. Express 25, 29927–29933 (2017).
- 45. Zhang, L. et al. Dual-periodically poled lithium niobate microcavities supporting multiple coupled parametric processes. *Opt. Lett.* **45**, 3353–3356 (2020).
- Dorrer, C., Roides, R., Bromage, J. & Zuegel, J. Self-phase modulation compensation in a regenerative amplifier using cascaded second-order nonlinearities. Opt. Lett. 39, 4466–4469 (2014).
- 47. Xiong, C. et al. Aluminum nitride as a new material for chip-scale optomechanics and nonlinear optics. *New J. Phys.* **14**, 095014 (2012).
- Zhu, D. et al. Integrated photonics on thin-film lithium niobate. Adv. Opt. Photonics 13, 242–352 (2021).
- Elshaari, A. W., Pernice, W., Srinivasan, K., Benson, O. & Zwiller, V. Hybrid integrated quantum photonic circuits. *Nat. Photonics* 14, 285–298 (2020).
- Lu, J., Li, M., Zou, C.-L., Al Sayem, A. & Tang, H. X. Toward 1% single-photon anharmonicity with periodically poled lithium niobate microring resonators. *Optica* 7, 1654–1659 (2020).
- Desiatov, B., Shams-Ansari, A., Zhang, M., Wang, C. & Lončar, M. Ultra-low-loss integrated visible photonics using thin-film lithium niobate. Optica 6, 380–384 (2019).
- Ilchenko, V. S., Savchenkov, A. A., Matsko, A. B. & Maleki, L. Nonlinear optics and crystalline whispering gallery mode cavities. *Phys. Rev. Lett.* 92, 043903 (2004).

Publisher's note Springer Nature remains neutral with regard to jurisdictional claims in published maps and institutional affiliations.

© The Author(s), under exclusive licence to Springer Nature Limited 2022

LETTERS NATURE PHYSICS

Methods

Device fabrication. Devices were fabricated from 1- μ m aluminium nitride grown on sapphire substrates using metalorganic vapour-phase epitaxy (MOCVD). FOx-16 resist was used for patterning photonic circuits with electron-beam lithography. After development with tetramethylammonium hydroxide (TMAH), plasma etching with Cl₂/BCl₃/Ar was used to transfer the pattern to the aluminium nitride layer. Finally, SiO₂ cladding was deposited by plasma-enhanced chemical vapour deposition (PECVD).

CAR measurement. When calculating the CAR, the coincidence count was averaged within the coincidence peak (±1 ns) at zero delay. The accidental count was estimated by averaging the coincidence count with a large time delay outside the peak.

Data availability

Source data are provided with this paper. All other data that support the plots within this paper and other findings of this study are available from the corresponding author upon reasonable request.

Acknowledgements

L.F. acknowledges support from the US Department of Energy, Office of Advanced Scientific Computing Research, (Field Work Proposal ERKJ355), the Office of Naval Research (N00014-19-1-2190), the National Science Foundation (ECCS-1842559, CCF-190791), the NSF Center for Quantum Networks, AFOSR (FA9550-21-1-0225) and the

II-VI foundation. C.C. acknowledges support from the National Science Foundation (ECCS-1842559). L.Z. acknowledges support from AFOSR (FA9550-21-1-0225). Device fabrication was performed in the OSC cleanrooms at the University of Arizona and the cleanroom of Arizona State University. Superconducting nanowire single-photon detectors are supported by NSF MRI INQUIRE.

Author contributions

C.C. and L.F. conceived the idea, designed the experiment and analysed the data. L.Z. designed and fabricated the device. C.C. derived the theoretical model and performed the measurement. L.F. supervised the work.

Competing interests

The authors declare no competing interests.

Additional information

Supplementary information The online version contains supplementary material available at https://doi.org/10.1038/s41567-022-01542-x.

Correspondence and requests for materials should be addressed to Linran Fan.

Peer review information *Nature Physics* thanks Thiago Alegre and the other, anonymous, reviewer(s) for their contribution to the peer review of this work.

Reprints and permissions information is available at www.nature.com/reprints.